ISSN 1330-3651 (Print), ISSN 1848-6339 (Online)
Received: 16 December 2024; Accepted: 14 September 2025

https://doi.org/10.17559/TV-20241216002197
Original scientific paper

Seismic Performances of Different Strengthening Techniques in Masonry Residential Buildings

Alper ÖZMEN

Abstract: This study evaluates the seismic performance and retrofitting strategies for a masonry residential building in Malatya, Türkiye, that collapsed during the February 6, 2023, Kahramanmaraş earthquake owing to an illegally added story. Nonlinear static (pushover) and dynamic (time history) analyses were performed using a finite-element macro-model. The unretrofitted structure collapsed at approximately 0.45 g in the longitudinal direction. Two retrofitting techniques, namely stainless steel strip jacketing and carbon fiber-reinforced polymer (CFRP) laminates, were investigated. The strengthened models demonstrated significantly improved seismic performance: the stainless steel strip retrofit increased the base shear capacity to 0.69 g, whereas the CFRP retrofitting further enhanced it to 0.79 g. Both methods also reduced the maximum inter storey drift ratios (from 0.50% to 0.34% for CFRP) and limited the crack widths (from 17.8 mm to less than 8 mm). CFRP retrofitting provided the most effective improvement. These results highlight the urgent need to retrofit unauthorized story additions in masonry buildings to enhance seismic resilience and inform policy decisions in seismically active regions.

Keywords: 2023 Kahramanmaras earthquakes; illegal added storey; masonry building; seismic retrofitting

1 INTRODUCTION

Türkiye frequently experiences earthquakes, which often result in severe damage and loss of life in affected areas. On February 6, 2023, the country was hit by two devastating earthquakes with magnitudes of 7.7 and 7.6, marking the most lethal seismic event in its history. These quakes claimed the lives of over 55,000 individuals and led to the collapse of more than 38,000 buildings, affecting 11 provinces and nearly 10 million residents. This unparalleled level of destruction underscores the seismic weaknesses of the current building infrastructure and emphasizes the critical need for enhanced design codes and effective retrofitting measures.

Various studies have been conducted to evaluate the damage or collapse of structures after the 2023 Kahramanmaras earthquakes. [1-7] investigated the causes of damage to reinforced concrete (RC) buildings in earthquake-affected areas. These studies highlight the need for improved building codes and retrofitting measures to enhance the seismic resilience of structures in Turkey. By identifying common vulnerabilities, researchers aim to mitigate future earthquake risks and protect populations from potential disasters. Various researchers have investigated masonry structures in earthquake-affected areas.

Işık et al. [8] examined the occurrence of earthquakes and the intensity of ground shaking, with a specific focus on the reasons for the collapse and failure of buildings constructed using unreinforced masonry. Structural damage was attributed to non-adherence to seismic design requirements, the presence of heavy mud roofs, inadequate connections, and substandard workmanship. Kahya et al. [9] investigated the seismic analysis of old masonry buildings in Hatay, Turkey, utilizing field observations and computer methods. The findings from the two seismic events that impacted Kahramanmaraş provide insights into the potential causes of damage. Numerical models provide insights into crack patterns and deterioration mechanics. Notwithstanding the significant destruction, a component collapsed in the Defne district. This study offers retrofitting suggestions to support reconstruction and rehabilitation operations and improve the comprehension of the seismic performance of masonry structures. Mercimek [10] examined the mechanisms of structural deterioration in masonry buildings following earthquakes in Kahramanmaraş, Turkey. The analysis included an assessment of the building inventory, ground acceleration, seismic characteristics, and damage patterns. This study examines the failure processes of out-of-plane and corner structures, which are primarily due to poor connections between the walls, roof, and floor; insufficient axial load; low material strength; subpar workmanship; and a lack of engineering service. Irregular door and window openings that exceed the standards trigger failure mechanisms inside the plane structure. This study also evaluated the benefits and drawbacks of enhancing techniques for masonry structures that have experienced light to moderate damage. Işık et al. [11] investigated the structural damages of 27 mosques and minarets in Adıyaman province, Turkey, during the February 6, 2023, Kahramanmaraş earthquakes. Despite the significant damage, no loss of life was experienced, and the main cause was the local masters' lack of engineering service.

The novel contribution of this study is its emphasis on the evaluation and retrofitting recommendations for illegally constructed additional stories in earthquake-prone regions. A thorough examination of the current literature reveals a substantial void in research pertaining to the seismic performance improvement of these unauthorized structures, which are frequently constructed without complying with regulatory requirements or obtaining the requisite approvals. The consequences of failing to address illegal construction in earthquake-prone areas can be devastating, as shown by past events that have resulted in widespread destruction and loss of life.

In Türkiye, the responsibility for retrofitting unauthorized floors primarily rests with property owners, whereas local municipalities, under the jurisdiction of the Ministry of Environment, Urbanization, and Climate Change, are tasked with oversight and enforcement. The "building amnesty" laws enacted in 2018-2019 conferred legal recognition upon numerous unauthorized extensions but did not mandate seismic retrofitting. Consequently,

most strengthening efforts are contingent on voluntary actions by owners unless a building is officially classified as unsafe. In such cases, municipalities have the authority to mandate retrofitting or even demolition. This regulatory framework highlights a significant discrepancy between legalization and safety, emphasizing the need for proactive measures to ensure that retrofitted illegal floors adhere to the minimum seismic performance standards.

By focusing on retrofitting recommendations for these structures, this study aims to fill a crucial gap in the existing research and provide valuable insights for authorities and building owners. It is essential for stakeholders to take proactive measures to ensure the safety and stability of these buildings to prevent future disasters from occurring.

This study selected a masonry building that collapsed after the 2023 Kahramanmaras earthquake as a case study. Pushover and time history analyses were conducted to determine the performance of the structure. The 2023 Kahramanmaras earthquake records were used for the nonlinear time history analyses. Nonlinear analyses were conducted using the finite element method (FEM) with DIANA FEA software. The performance of the structure was evaluated according to the FEMA 356 standard.

2 DESCRIPTION OF THE CASE STUDY STRUCTURE

The case study structure is located in Malatya, Türkiye. The location of the building is shown in Fig. 1. When the researchers reached the location of the building after the 2023 Kahramanmaraş earthquake, the building had completely collapsed (Fig. 2).

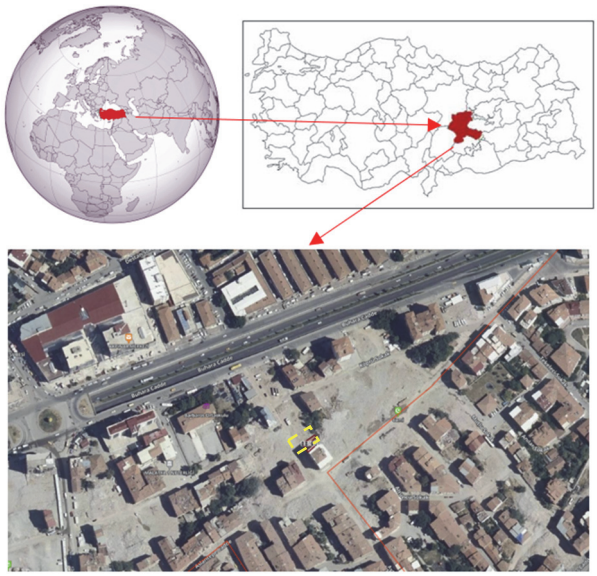

Figure 1 Location of the building

The building was constructed with masonry using clay bricks and consisted of three stories, each 3 m in height. The outer walls were 30 cm thick, whereas the inner walls varied in thickness from 20 cm to 10 cm. The architectural plan of the building includes two balconies positioned in the designated areas. The Google Maps images captured before the 2023 Kahramanmaras earthquake reveal an additional story that was not accounted for in the original architectural plans of the building (Fig. 3).

a) b)

Figure 2 State of the building a) Before earthquake; b) Post-earthquake

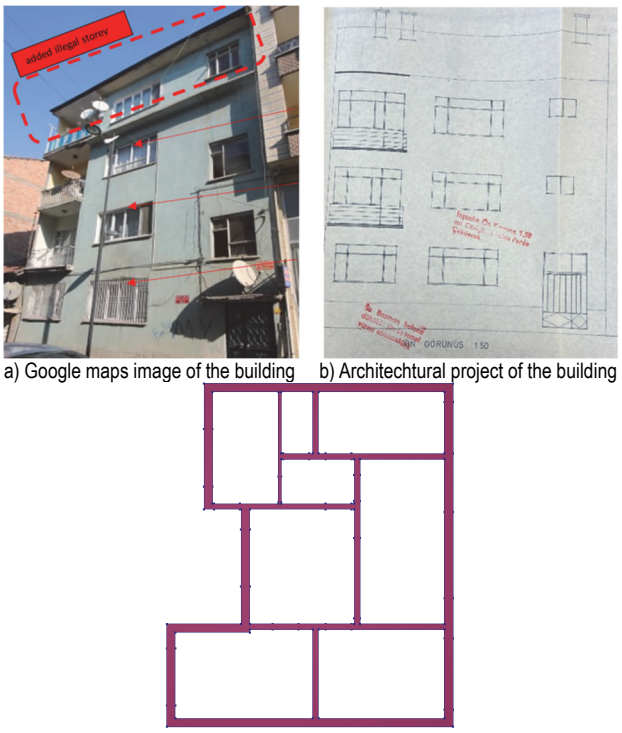

a) Google maps image of the building b) Architechtural project of the building

c) Architectural plan

Figure 3 The architechtural plan of the building and illegal storey addition

2.1 Material Properties of the Building

The clay bricks used in the construction of the masonry walls were found to have dimensions of 190 × 90 × 60 mm, with material properties detailed in Tab. 1 [12]. The sample was taken from the debris following the earthquake to analyze its composition and strength. The debris and clay brick samples taken from the building can be seen in Fig. 4.

Table 1 Some properties of clay brick

Weight / kg/pc	γ / kg/m^3	Thermal conductivity / W/mK	f_c / MPa	ft / MPa	ν
1.4	2100	1.07	5	0.6	0.20

Utilizing the finite element method (FEM), three distinct modeling approaches have been devised for historic masonry structures, namely macro modeling techniques, simple micro modeling, and detailed micro modeling. Illustrative diagrams of these methodologies are presented in Fig. 5. The macro modeling technique, as described by [13], was employed in the present study. This method considers masonry as a composite material, with

no distinction between mortar connections and bricks or stones. The macro modeling technique is well-suited for large-scale structural models due to its lower computing requirements [14-16].

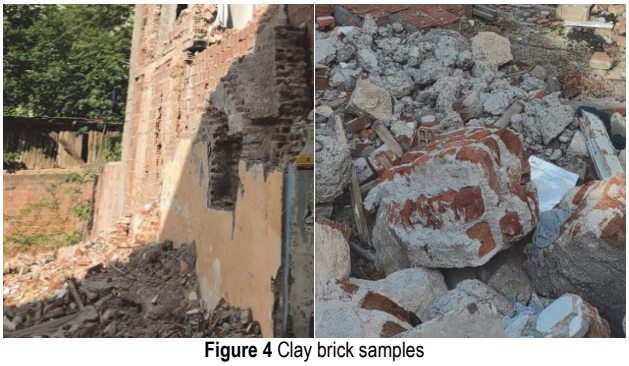

Figure 4 Clay brick samples

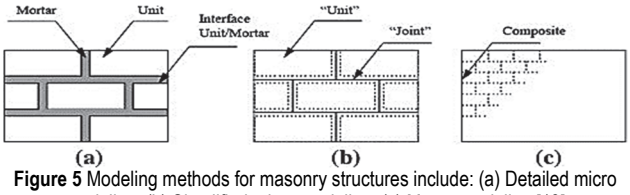

Figure 5 Modeling methods for masonry structures include: (a) Detailed micro modeling; (b) Simplified micro modeling; (c) Macro modeling [13]

The main difficulty is ascertaining the homogeneous material characteristics of the masonry. Before making this decision, it is necessary to answer two important questions: the characteristics of the mortar and a choice of the suitable equation for calculating the average material properties of the brickwork [17]. Clay brick samples from earthquake debris were tested for their physical properties. No intact mortar fragments could be recovered for testing, as the mortar was crushed during collapse. Without official technical documentation of the building, except for Google Maps images and a partial architectural plan, the structural model was reconstructed using field measurements, photographs, and standard regional construction practices.

Due to the lack of information regarding mortar, assumptions were made based on the extant literature, resulting in a mortar compressive strength of 1 MPa and a Poisson's ratio of 0.05. A range of compressive strengths is presented in the pertinent literature, with cited values ranging from 1 MPa to 6 MPa [18-20]. In this research, the finite element model was developed using the macro modeling approach, wherein both mortar and stone are represented as a single material. Hence, some empirical formulas recommended by different researchers and standards were used to determine the composite material properties [21].

For determining the compressive strength of masonry units, Eq. (1) as proposed by Proske and Van Gelder (2009) is utilized. This equation calculates the strength based on the compressive strengths of both the mortar and stone.

$$f_{c,\mathrm{mas}} = a f_{c,\mathrm{sto}}^{b} f_{c,\mathrm{mor}}^{c} \tag{1}$$

In this equation, $f_{c,\mathrm{mas}}$ represents the compressive strength of the homogenized masonry unit, a is the classification coefficient for the masonry unit, and b and c denote the volumetric ratios of stone/brick and mortar, respectively.

These coefficients are specified in Eq. (2), which is derived from Eq. (1), as cited by Ril 805 (2007). Additionally, consistent with findings from previous research, the tensile strength of the masonry unit is assumed to be 1/10 of its compressive strength [21, 24-26].

$$f_{c,\mathrm{mas}} = 0.6_{c,\mathrm{sto}}^{0.70} f_{c,\mathrm{mor}}^{0.30} \tag{2}$$

The Poisson's ratio and density of the masonry were calculated using Eqs. (3a) and (3b) proposed by Ersoy (2001).

$$\gamma_{\mathrm{mas}} = \gamma_{\mathrm{brick}} \cdot V_{\mathrm{brick}} + \gamma_{\mathrm{mortar}} \cdot V_{\mathrm{mortar}} \tag{3a}$$

$$v_{\mathrm{mas}} = v_{\mathrm{brick}} \cdot V_{\mathrm{brick}} + v_{\mathrm{mortar}} \cdot V_{\mathrm{mortar}} \tag{3b}$$

V_{brick} and V_{mortar} are the volume fractions of the stone and mortar, respectively. The modulus of elasticity for the masonry unit was determined as $E_{\mathrm{mas}} = 1000 f_c$, as recommended by EN 1996-1-1 [28]. The homogenized material properties of the building are listed in Tab. 2.

Historical masonry structures typically exhibit linear behavior under low load levels but may demonstrate nonlinear behavior when subjected to loads that exceed a certain threshold. This nonlinear behavior in structural materials primarily arises from tensile forces induced by seismic activities in historic constructions. Various nonlinear material models are available for masonry structures in different finite element software packages. DIANA FEA software was used for the analyses in this study. The Total Strain-Based Crack Model (TSBCM) is the predominant material model used in the DIANA FEA software for simulating masonry structures. This material model, which was originally proposed by Vecchio and Collins (1986), is widely used in the analysis of reinforced concrete structures subjected to shear and normal stresses. It incorporates the effects of concrete cracking, tension stiffening, and compression softening to provide a more accurate representation of the concrete behavior under complex loading conditions.

In the Total Strain-Based Crack Model (TSBCM) method, cracking is treated as a distributed effect along a single direction, and the material exhibiting cracks is modeled as a continuous medium possessing anisotropic properties, as stated in the DIANA FEA (2022). For example, in a simulation of a historical masonry building undergoing seismic loading, the TSBCM in the DIANA FEA software accurately predicted the formation and propagation of cracks in the structure. By considering cracking as a distributed effect and modeling the material as anisotropic, engineers can assess the structural integrity and safety of buildings under various loading conditions.

The TSBCM utilized in DIANA FEA software delineates the behavior of materials under both tensile and compressive stresses through a unified stress-strain relationship. Within the TSBCM, various methods, such as elastic, constant, and parabolic models, are used to conceptualize the behavior under tension and compression. The parabolic model is chosen for this study due to its specific characteristics, as illustrated in Fig. 6 [31]. The parameters essential for implementing the Total Strain-Based Crack Model include density (ρ), elastic modulus

(E), Poisson's ratio (v), compressive strength (f_c), compressive fracture energy (G_c), tensile strength (f_t), and mode-1 fracture energy (G_f).

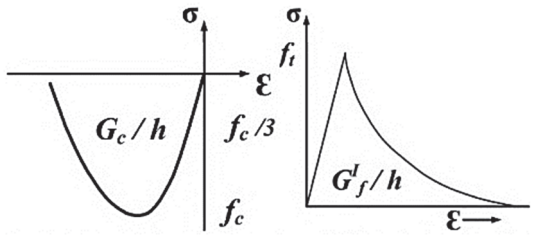

Figure 6 Typical behaviour of the TSBCM under compressive (left) and tensile stress (right) [30]

The nonlinear behavior of the Total Strain-Based Crack model is controlled by the fracture energy dissipation criteria, indicated as G_f and G_c. The manner in which the model manages the energy released during fracturing under tensile and compressive conditions, respectively, is determined by these parameters [32]. The fracture energies in tension and compression are defined by Eqs. (4a) and (4b), respectively.

$$G_f = 0.025\left(2f_t\right)^{0.7} \tag{4a}$$

$$G_c = df_m \tag{4b}$$

f_t and f_m are the tensile and compressive strengths of the masonry, respectively. Parameter d represents the ductility index and is defined by Eq. (4c).

$$d = 2.8 - \left(0.1f_m\right) \tag{4c}$$

The linear and nonlinear homogenized material properties of the case study structure are presented in Tab. 2.

Table 2 Homogenized mechanical properties of finite element model of the building

Property	Value
E / MPa	1850
Fc / MPa	1.85
Ft / MPa	0.19
$\gamma_{yığma}$ / g/cm^3	2.04
v	0.16
Gc	4.85
Gf	0,0125

3 FINITE ELEMENT MODELING OF THE BUILDING

A finite element model (FEM) was created using the DIANA FEA finite element software [30]. In the finite element analysis of the structure, HX24L, PY15L, TE12L, and TP18L elements were employed.

The finite element model of story-added building consists of 17672 solid HX24L, PY15L, TE12L, TP18L elements, and 27532 nodes. In the structural finite element analysis, the elements HX24L, PY15L, TE12L, and TP18L were utilized. The HX24L is a 24-node, three-dimensional isoparametric solid brick element, employed for modeling masonry walls. The PY15L is a 15-node interface element crafted to simulate potential separation or sliding between adjacent parts. The TE12L is a 12-node triangular surface element that is often used to represent irregular boundaries or thin components. The TP18L is an 18-node quadratic thick shell element, ideal for modeling floors and slabs. These elements were integrated to effectively capture the nonlinear behavior of masonry, interface discontinuities, and slab responses within a unified macro-model framework.

A mesh sensitivity analysis was carried out to determine the optimum mesh size suitable for masonry and soil elements. The mesh sizes were decided to be 35 cm for the masonry elements. The FEM model of the structure was given in Fig. 7. The control node for the pushover and nonlinear time history analyses (NLTHA) is marked in Fig. 7. In the pushover analyses, several control points were found, and only one control point with the lowest capacity was chosen for both the pushover and NLTH analyses. To maintain brevity, these findings are not presented in this paper.

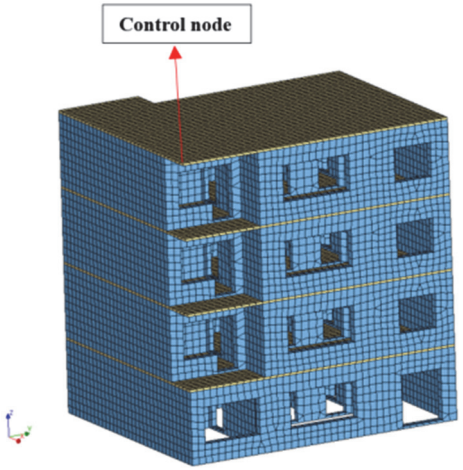

Figure 7 FEM of building

4 ANALYSIS RESULTS OF UNREINORCED STATE OF THE BUILDING

In this section of the study, modal, pushover, and nonlinear time history analyses were performed, and the results were compared.

4.1 Modal Analyses

A modal (eigen frequency) analysis was conducted using a three-dimensional finite element model (FEM) to evaluate the dynamic behavior of the structure. This analysis reveals the deformed shapes associated with effective vibration modes, which are defined by their mass participation ratios (MPR) and corresponding periods [33]. The first 3 mode shapes and vibration frequencies of the finite element model of the structure are displayed in Fig. 8. Mode 1 is translation in the y direction, Mode 2 is translation in the x direction, and 3rd mode is torsion. The highest effective MPR (67.1 %) in the x direction was obtained in the 2nd mode. In the y direction, the highest effective MPR (74.8 %) was obtained in the 1st mode. The higher effective MPR values in the y-direction for the building suggest that the lateral stiffness in that direction is stronger.

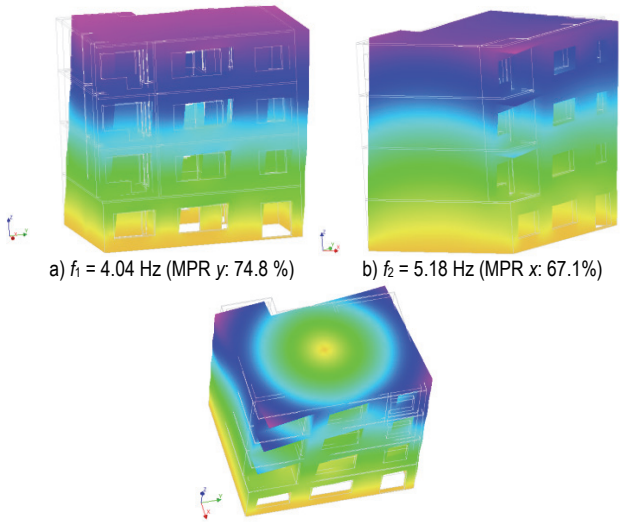

a) f_1 = 4.04 Hz (MPR *y*: 74.8 %) b) f_2 = 5.18 Hz (MPR *x*: 67.1%)

c) f_3 = 6.79 Hz (MPR *x*: 0.08%/ MPR *y*: 0.06%/ MPR *z*: 0.03%)

Figure 8 First 3 Mode shapes and frequencies of the structure (MPR: mass participation ratio)

4.2 Pushover Analyses

To ascertain the lateral load-bearing capacity of the buildings, pushover analyses were performed in both the transverse and longitudinal directions. The foundational principle of this method relies on nonlinear computations designed to assess the seismic response of structures subjected to applied forces. This approach fundamentally involves the application of incremental horizontal forces to structures, escalating these forces until a predetermined limit value is reached. In this study, modal pushover analysis (MPA) was performed. The MPA, introduced by Chopra and Goel (2002) for multi-storey frame structures, employs a pushover analysis that utilizes force distributions aligned with a single mode of vibration. The modal pushover analysis enables the comprehension of the structural reaction to horizontal stresses and the corresponding causes of damage. First, a modal analysis was performed to determine the modes with the largest mass participation rates. Subsequently, the allocation of horizontal loads to be imposed on the structure is calculated, as indicated by Eq. (5).

$$s_n^* = M\phi_n \tag{5}$$

In the above Eq. (5), M represents the mass matrix, and ϕ_n represents the mode shape of the n^{th} mode. This method involves applying loads to the structure in a monolithic manner and gradually increasing the loads until structural collapse occurs. This technique produces a base shear force curve relative to the displacement at a certain control point on the structure. This curve, known as the capacity curve, helps determine the structure's load-bearing capacity under horizontal loads [35]. For the structures being studied, nonlinear static analyses were used to obtain curves that show how the base shear force-to-building weight ratio (V_t/W) changed with respect to the control node displacement. There are different studies on the selection of control nodes. It was suggested that the control points should be selected at high points on the macroblocks, where the collapse mechanism is likely to occur [36]. The nonlinear static results (capacity curves) were derived from the control node (Fig. 7) in the transverse and longitudinal directions, as shown in Fig. 9.

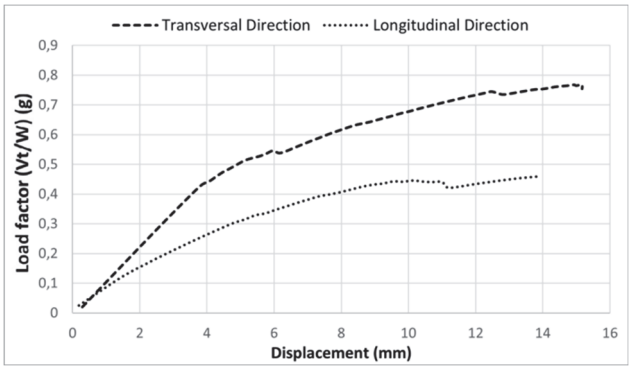

Figure 9 Capacity curves of the building

Pushover analysis graphs are shown in Fig. 9 for the transverse and longitudinal directions. According to the results of the nonlinear static analysis, a building with an added story resists a maximum of 0.76 g in the transverse direction. In the longitudinal direction, the building resisted a maximum of 0.45 g. After the nonlinear static analyses, the crack propagations are shown in Fig. 10. Furthermore, the damage patterns of the building were evaluated using the maximum crack widths, which are considered reliable damage indicators [37]. Cracks were visible on all floors of the building. We observed that these cracks were concentrated on the edges of the window openings and the 10 cm-thick interior walls. The concentration of cracks along the edges of the window openings and interior walls indicates potential weak points in the structure that may be susceptible to further damage or collapse.

The maximum crack widths of both buildings are presented in Fig. 10. The crack widths were obtained in the last step before collapse. For the building, the maximum crack width observed was 11.05 mm in the transversal direction and 11.01 mm in the longitudinal direction.

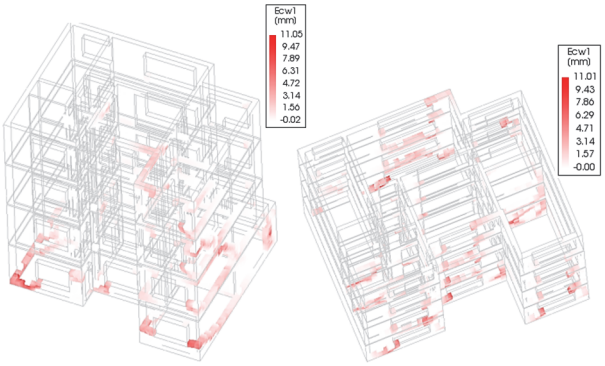

a) Transversal direction b) Longitudinal direction

Figure 10 The maximum crack widths

4.3 Nonlinear Time History Analyses

Nonlinear time history analyses (NLTHA) have been carried out on the finite element models to examine how the structure behaves during an earthquake. Six different earthquake records (2023 Kahramanmaras earthquakes and 2020 Sivrice earthquake) have been selected for the nonlinear analyses. The analyses employed an effective 15-seconds of the seismic records. The earthquake

accelerations applied to the structure in the *y* direction (longitudinal direction). Before the NLTHA, a pushover analysis was performed in both horizontal directions (*x*, *y*). According to the pushover results, the *y* direction (longitudinal) was found to be the weak direction of the structure. Also, vertical ground accelerations have not been taken into account in the analyses. The earthquake records used in the analysis were taken from the Turkish Acceleration Data and Analysis System [38]. Rayleigh damping proportional to mass and stiffness is used in NLTHAs. The damping ratio is considered as 5% as recommended in similar studies [15, 18, 20].

The frequency characteristics of an earthquake have a significant impact on the seismic response of a structure. Important measurements for assessing the frequency characteristics of seismic occurrences include the dominant period, average period, intensity of the power spectrum, and the ratio of peak ground acceleration (PGA) in g units to peak ground velocity (PGV) in meters per second. The inclusion of these criteria is crucial in order to conduct a thorough evaluation of the effect of an earthquake on the structural stability [39, 40]. The PGA/PGV ratio is a straightforward and informative measure for analyzing the frequency characteristics of an earthquake. Earthquake motions are categorized into three groups based on the ratio of peak ground acceleration (PGA) to peak ground velocity (PGV). A ratio larger than 1.2 indicates a high frequency content, a ratio between 0.8 and 1.2 suggests an intermediate frequency content and a ratio less than 0.8 signifies a low frequency content. This classification system simplifies the interpretation of seismic data by providing a distinct structure to comprehend the frequency characteristics of earthquake movements [41].

The frequency content of earthquakes is evaluated by using the ratio of PGA to PGV. As shown in Tab. 3, 2023 Kahramanmaras Pazarcık (4614), 2023 Kahramanmaras Elbistan (4406), 2023 Malatya Doğanşehir earthquakes are high, 2023 Kahramanmaras Nurdağı earthquake is intermediate, 2023 Kahramanmaras Pazarcık (4408) and 2020 Elazığ Sivrice earthquakes are low frequency motions. The selection of earthquake records adhered to the guidelines established by the Turkish Building Earthquake Regulation of 2018 [42]. Consequently, the earthquake records intended for time history analyses must be scaled in accordance with the horizontal elastic design spectrum. This scaling is based on the geographical coordinates of the structure, the local soil classification, and the designated level of earthquake ground motion. The coordinates of the building are 38.35313°, 38.3234°. The soil class was determined to be ZC in accordance with the soil survey reports obtained close to the location of the chosen building. ZC is associated with medium-stiff soils, characterized by shear wave velocities ranging from 360 to 760 m/s, and typically includes sandy clays or silty sands, which offer moderate stiffness and damping properties. The construction site falls under the ZC soil classification, as identified by nearby geotechnical survey reports in line with the Turkish Building Earthquake Code (2018). This classification was utilized to establish the seismic input spectrum and to scale earthquake records.

The Seismomatch software was utilized to scale the earthquake records employed in this study [43]. Additionally, Tab. 3 offers comprehensive details regarding the earthquakes chosen for the analysis. Fig. 11 presents the scaled acceleration-time graphs for these selected earthquakes.

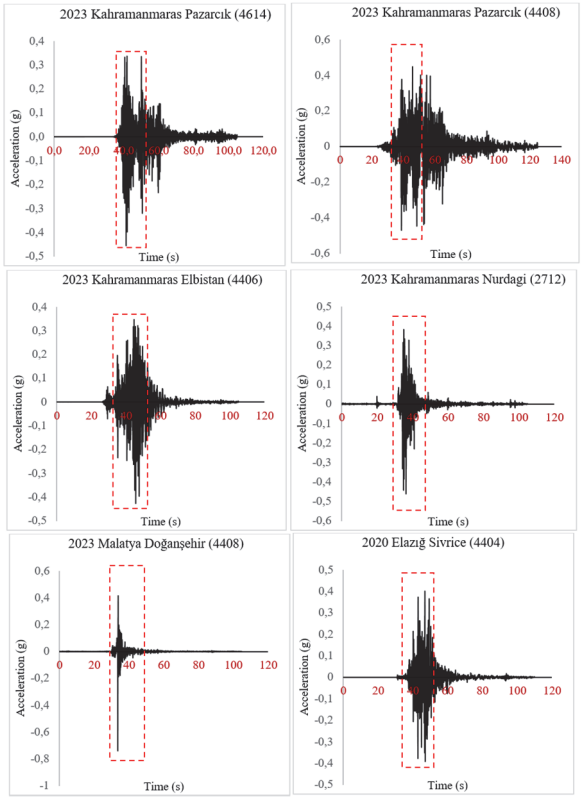

Figure 11 Scaled earthquake acceleration plots

The spectral acceleration plots in Fig. 12 show the comparison between the target elastic design spectrum and the acceleration spectrum of the selected earthquake records. It is evident that three of the seismic responses in all records exceeded the design spectrum with a return period of 475 years. Specifically, the 2023 Kahramanmaraş Pazarcık record (Station code 4614), the 2023 Kahramanmaras Elbistan record (Station code 4406), and the 2023 Kahramanmaras Nurdağı record (Station code 2712) all surpassed the specified design criteria.

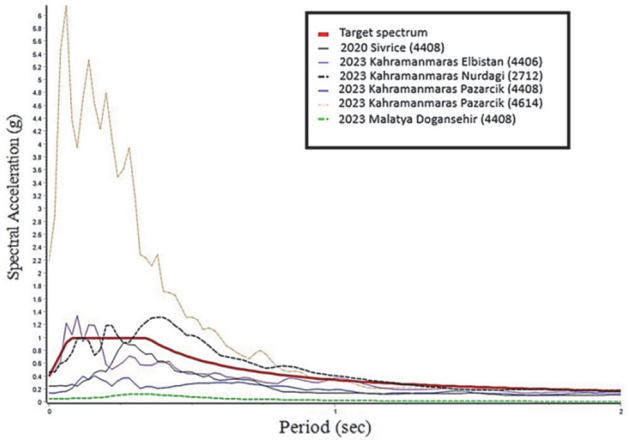

Figure 12 Target design spectrum and spectral accelerations

The selected records' time series was utilized in all models by the Newton-Raphson time integration method with a time step of 0.01 s. The mass and stiffness

proportional (Rayleigh) damping model was utilized to solve the equilibrium equations. Rayleigh damping was incorporated into the dynamic calculations, with a damping ratio of 5% selected based on previous research conducted by [44-46]. The Rayleigh damping coefficients were computed using Eqs. (6a) and (6b).

Table 3 Selected earthquake records

No	Earthquake	Record Station/ Horizontal Direction	Magnitude / M_w	Scale Factor	PGA / g	PGV / m/s	PGA/PGV	Distance / km	V_s / m/s
1	2023 Kahramanmaras Pazarcık	4614/ E-W	7.7	0.20	0.43	0.25	1.72	31.42	541
2	2023 Kahramanmaras Pazarcık	4408/ E-W	7.7	3.36	0.47	1.78	0.26	116.59	655
3	2023 Kahramanmaras Elbistan	4406/ N-S	7.6	0.97	0.46	0.28	1.64	70.17	815
4	2023 KahramanmarasNurdağı	2712/ N-S	6.6	1.07	0.48	0.38	1.20	21.27	599
5	2023 Malatya Doğanşehir	4408/ E-W	5.6	14.6	0.73	0.32	2.28	21.05	655
6	2020 Elazığ Sivrice	4404/ E-W	6.8	1.79	0.43	0.57	0.75	24.55	1382

$$a_0 = \xi \frac{2w_i w_j}{w_i + w_j} a_1 = \xi \frac{2}{w_i + w_j} \quad (6a)$$

$$C = a_0 M + a_1 K \quad (6b)$$

The equation involves the damping ratio ξ, the angular frequency w_i acquired in the i-th mode, and the angular frequency w_j obtained in the j-th mode. The damping matrix C is derived by using Eq. (6b) with the coefficients computed in Eq. (6a).

The maximum interstorey drift ratio is calculated by dividing the maximum interstorey drift by the height of the building. These parameters are crucial in assessing the structural performance of the building under seismic loading. The results of these evaluations can help engineers determine the adequacy of the building's design and make any necessary modifications to improve its seismic resistance. The displacement measurements resulting from the NLTHA were acquired from the Control Point (CP) depicted in Fig. 7. In the pushover studies discussed in Section 4.2, several control points were used. The control point for NLTH was determined by selecting the location where the greatest displacements occurred. In order to be concise, these findings are not displayed in this document. Also, the interstorey drift ratios were graphed using the nodes shown in Fig. 13. Each story levels were identified in order to obtain the drift ratios. The NLTH results are summarized in Tab. 4.

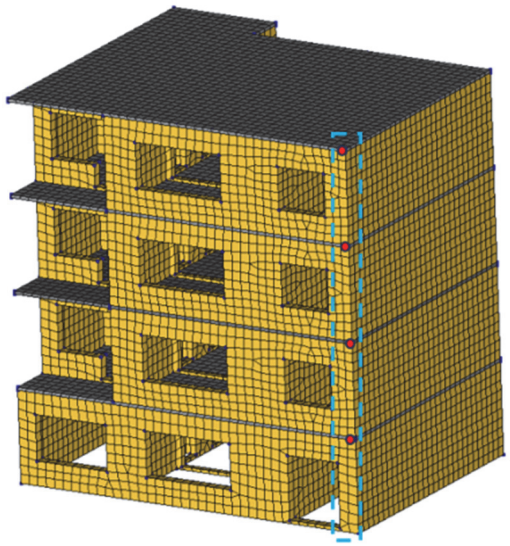

Figure 13 Considered nodes for story drift ratios

Relative story drifts are one of the most important parameters in evaluating buildings' performance. The seismic performance of the historical structure is categorized into different levels based on its ability to withstand earthquakes. These levels are Immediate Occupancy (IO), Life Safety (LS), and Collapse Prevention (CP) for the protection of human life and use. In this research, the maximum inter-storey drift ratio (ISDR) is utilized as the demand parameter for evaluating the performance of unreinforced masonry (URM) walls. According to FEMA 356, the acceptance limits for bed-joint sliding are set at IO = 0.10%, LS = 0.30%, and CP = 0.40%; thus, ISDR values are directly compared to these benchmarks. "Normalized displacement" results are presented solely for comparative graphing purposes; the performance assessment relies entirely on the maximum ISDR. Consequently, decisions regarding IO/LS/CP are based on the maximum ISDR.

The performance of the structure was then evaluated using the acceptance criteria specified for URM walls in the FEMA 356 standard, as outlined in Tab. 5.

Table 5 The acceptance criteria specified in FEMA 356 [47]

Standard	Limiting behavioral mode	Primary members		
		Immediate occupancy (IO) / %	Life safety (LS) / %	Collapse prevention (CP) / %
FEMA 356	Bed-Joint sliding	0.1	0.3	0.4

Based on the acceptance criteria, original project between the Life safety (LS) and Collapse prevention (CP) performance levels (significant but restorable damage), while the responses of the story added building remained above the Collapse prevention (CP) performance level (near collapse). According to the acceptance criteria detailed in Tab. 5, the building's average maximum ISDR is 0.50%, which surpasses the FEMA 356 CP threshold of 0.40%. This suggests a near-collapse or CP exceedance, aligning with the actual collapse observed following the earthquakes on February 6, 2023.

In reality, the structure has completely collapsed after the earthquake. These findings highlight the importance of adherence to FEMA 356 standards for ensuring structural safety and resilience in the face of seismic events.

Maximum response amplitudes were obtained under 2023 Malatya Doğanşehir earthquake (4408). Thus, the crack widths were presented under 2023 Malatya Doğanşehir earthquake.

Table 4 NLTHA results for buildings

	2023 Kahramanmaras Pazarcık (4614)	2023 Kahramanmaras Pazarcık (4408)	2023 Kahramanmaras Elbistan (4406)	2023 Kahramanmaras Nurdağı (2712)	2023 Malatya Doğanşehir (4408)	2020 Elazığ Sivrice (4404)	Average of six earthquakes
Normalized displacement / %	0.29	0.26	0.35	0.28	0.36	0.28	**0.30**
Crack width / mm	11.1	16.02	30.88	11.81	15.24	21.63	**17.78**
Max. inter story Drift ratio / %	0.5	0.47	0.61	0.52	0.48	0.42	**0.50**

When the performance of the structure was evaluated according to FEMA 356, it was observed that the pre-collapse performance level of the structure appeared. Considering the current condition of the building after the 2023 Kahramanmaraş earthquakes (the building collapsed), it was revealed that the numerical analyses were compatible with the current condition of the structure. Therefore, it was concluded that the structure should be strengthened.

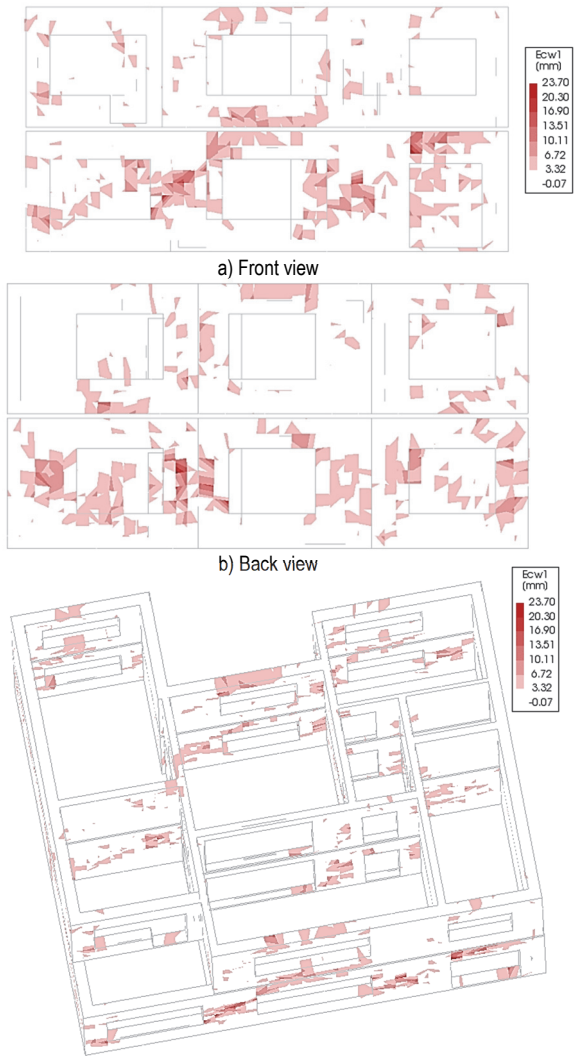

a) Front view

b) Back view

c) Isometric view

Figure 14 The crack widths of story added building under 2023 Dogansehir earthquake (3.96 s)

The crack widths of the building were given in Fig. 14. The crack widths were obtained under 2023 Doğanşehir earthquake (3.96 s). In the figure, the cracks range between 10-23 mm occurred under the earthquake. The crack widths observed during the 2023 Doğanşehir earthquake highlighted the potential vulnerabilities of the building under seismic activity. It was clear that immediate action needed to be taken to ensure the safety and stability of the structure in the event of future earthquakes. Fig. 15 highlights walls with significant cracks, which in this study are defined as those wider than 10 mm. These cracks, recorded during the 2023 Doğanşehir earthquake, measured between 10 and 23 mm. The walls with these cracks were identified as critical weak points and were chosen for retrofitting.

These walls will be reinforced in the retrofitting application. The structural engineers recommended using steel reinforcement and carbon fiber wrapping to strengthen the walls and prevent further damage in case of future seismic events. The retrofitting process would involve carefully assessing the building's weak points and implementing measures to enhance its overall stability. By addressing these vulnerabilities promptly, the building would be better equipped to withstand potential earthquakes and ensure the safety of its occupants.

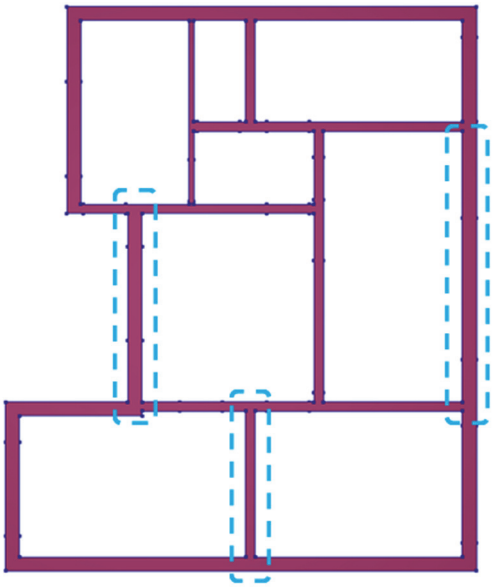

Figure 15 Retrofitting plan of the building

5 RETROFITTING APPROACH

The technical actions necessary to restore a structure to its original condition before an earthquake are referred to as "Repair". When the technical procedures and interventions in the structural system enhance the ability of a building to withstand earthquakes by improving its strength and ductility, this is referred to as "strengthening" or "retrofitting". The seismic response of a structure is determined by the interdependence of its structural elements, as well as the individual elements' strength, stiffness, and ductility [48]. Therefore, nearly all the efforts to reinforce URM buildings before earthquakes have

focused on strengthening the individual structural elements of masonry buildings, particularly walls that are prone to damage during seismic events. Additionally, there have been broader measures implemented to enhance the overall structural stability of the buildings.

Various retrofitting methods are described in the literature to enhance the seismic resistance of masonry walls. Some examples of materials used in construction include FRP textiles, stainless steel strips, steel bars, textile reinforced mortar, and steel grid systems. These materials are used to reinforce walls and improve their ability to withstand the lateral forces generated by earthquakes. In addition to strengthening individual elements, measures such as adding diagonal bracing, installing base isolators, and improving the foundation can help to increase the overall stability of URM buildings. By implementing a combination of these methods, engineers can help to ensure that these structures are better prepared to withstand seismic events and protect the lives of those inside.

This research examines a masonry retrofitting technique presented by [49] and CFRP reinforced technique. The study evaluates the effectiveness of these techniques in enhancing the seismic performance of URM buildings. By comparing the results of both methods, engineers can determine the most suitable retrofitting approach for improving the resilience of these structures.

5.1 Stainless Steel Strips Retrofitting

The investigation of [49] focused on the reinforcing technique of connecting stainless steel strips to unreinforced masonry walls. This method has been found to greatly improve both the ability of the masonry wall to withstand deformation and its load-bearing capacity. This technology successfully combines the durability of stainless steel with the structural characteristics of masonry, resulting in enhanced resistance to mechanical pressures. The retrofitting procedure is illustrated in Fig. 16.

Figure 16 Visual representation of retrofitting technique adopted from [49]

5.1.1 Verification of the Recommended Retrofit Model

The retrofitting approach described above was employed to enhance the seismic resistance of the structure in the case study. Therefore, it is necessary to validate the numerical model of the retrofitting approach by experimental investigation. The numerical model was validated using the experimental data obtained by [49]. The experimental system was simulated using the 3D Finite Element Method. The 3D FEM utilized the macro modelling approach. The DIANA FEA software was utilized in the finite element model of the wall. The wall's nonlinear material behavior was modeled using the Total Strain Base Crack model. Section 3 contains comprehensive information on the whole strain base crack model. The wall's linear material characteristics were obtained from Jin et al. (2023). The approach outlined in Section 3 was used to calculate the nonlinear material characteristics. The wall's nonlinear material characteristics are outlined in Tab. 6.

Table 6 Homogenized material properties of verification FEM

Property	Wall	Steel strips
E / MPa	1500	200000
Fc / MPa	1.5	-
Ft / MPa	0.15	565
$\gamma_{masonry}$ / g/cm^3	2.0	7.85
v	0.25	0.30
Gc	2.40	-
Gf	0.0107	-

A mesh sensitivity analysis was conducted by examining different element sizes. For the local retrofitted wall model (Fig. 18), a finer mesh of approximately 10-12 cm was used, to accurately represent the interaction between the masonry and the retrofitting components. Although the detailed results of the sensitivity analysis are not included here to keep the manuscript concise, they verified the appropriateness of the chosen mesh sizes. Concerning the retrofitting system, parameters were derived from the validated experimental study by Jin et al. (2023) on specimens MW1 and RMW1. In that research, stainless steel strips measuring 16 mm in width and 0.5 mm in thickness (tensile strength ≈ 565 MPa) were placed at horizontal intervals of 325-350 mm and vertical intervals of 310-340 mm. These values, shown to effectively enhance the in-plane shear resistance of masonry walls, were directly applied in our numerical model to align with experimental findings. In the numerical model, the steel strip mesh was attached to the masonry wall under the assumption of a rigid contact, meaning a perfect bond. This method assumes that there is no relative movement or separation between the strip elements and the wall surface, allowing for complete stress transfer. This simplification is frequently used in previous studies on masonry retrofitting and offers conservative estimates of the strengthening effectiveness.

Initially, the specimen without reinforcement (MW1) and reinforcement specimen (RMW1) was simulated. A comparison was made between the experimental and numerical results. Fig. 17 displayed a 3D model and experimental setup.

Finite element models of MW1 and RMW1 were given in Fig. 18.

Tab. 7 displays the maximum displacement and maximum force of both the experimental wall and the computational findings. Furthermore, Fig. 19 provided displacement-load curves for both the MW1 and RMW1. Based on the findings, there is a disparity of 23.1% and 17.1% between MW1 and the numerical values for displacement and force, respectively. In addition, the disparity between RMW1 and the enhanced numerical outcomes is 7% and 3% for displacement and force, correspondingly.

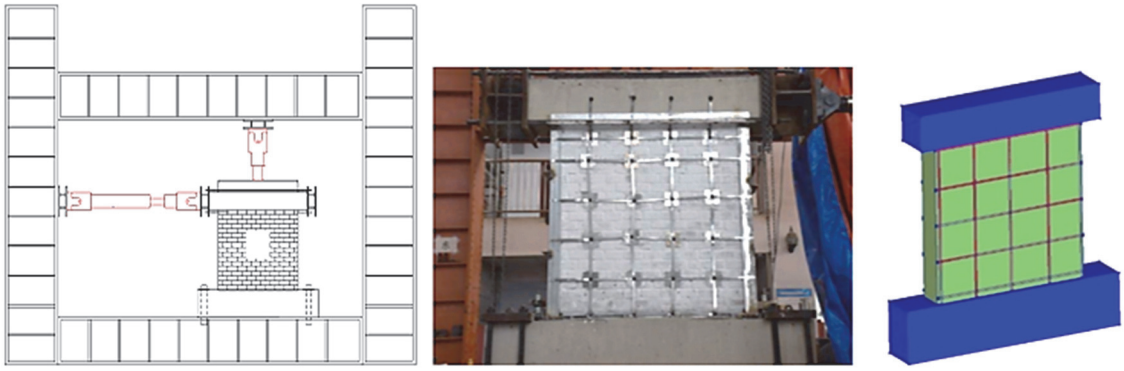

Figure 17 3D model and experimental system [49]

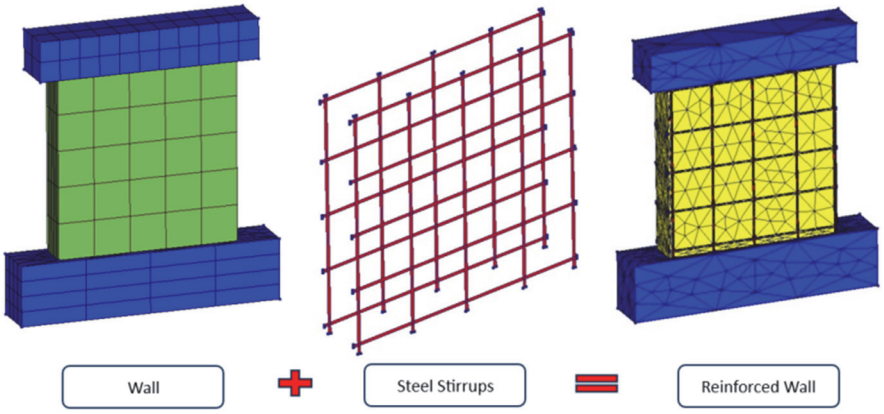

Figure 18 Finite element models of experimental system

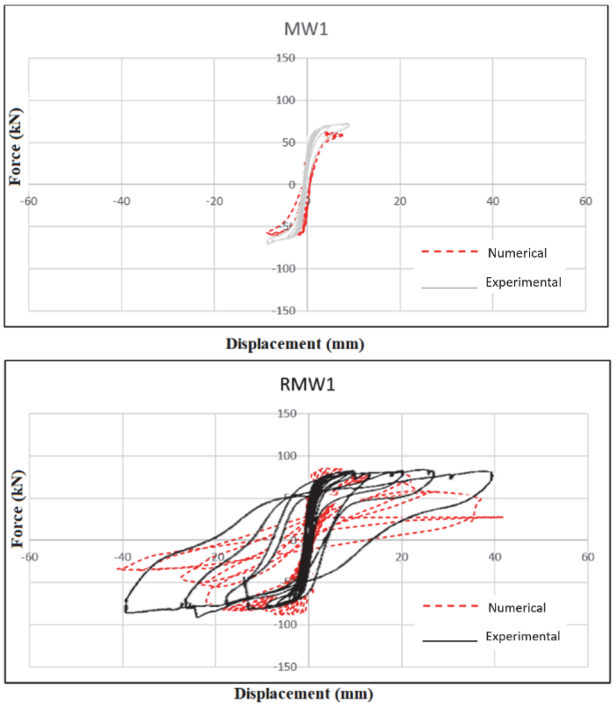

Figure 19 Force- displacement curves for unreinforced and reinforced walls

Table 7 Comparison of experimental and numerical results

MW1 (Unreinforced wall)			
	Experimental	Numerical	Difference
Peak displacement / mm	14	10.76	23.1 %
Peak Force / kN	75.31	62.41	17.1 %
RMW1 (Reinforced wall)			
	Experimental	Numerical	Difference
Peak displacement / mm	38.85	41.6	7 %
Peak Force / kN	87.54	84.8	3 %

5.2 Application of CFRP Reinforcement

Over the last twenty years, there has been a growing trend in using Fiber Reinforced Polymer (FRP) composites, specifically unidirectional strips, to strengthen and renovate historical masonry structures.

While FRP retrofitting offers the greatest enhancement in strength and reduction of drift, it comes with significant limitations. The process demands meticulous surface preparation and skilled labor, as inadequate bonding can lead to early failures. The high costs associated with materials and installation might restrict its use in low-income housing projects. Additionally, FRP offers limited defense against out-of-plane failures unless anchors are used and requires protective coatings due to its vulnerability to fire. These considerations suggest that the application of FRP should be assessed within the context of economic and safety limitations.

Figure 20 Some examples of CFRP applications [50, 51]

A significant amount of experimental research has been conducted to study the overall behavior of masonry structures reinforced with FRP. Thus, this study proposes the use of CFRP (Carbon Fiber Reinforced Polymer) for

on-site implementation, allowing for customization during procurement to ensure compatibility with masonry texture. In addition to its high mechanical strength, CFRP offers benefits such as resistance to chemical agents, impermeability to water, and reversibility. Some examples of CFRP application can be seen in Fig. 20.

Verification of Retrofitting Technique

The aforementioned retrofitting method was utilized to improve the seismic resilience of the structure in the specified case study. Hence, it is imperative to verify the accuracy of the numerical model for the retrofitting method by experimental analysis. The numerical model was verified using the experimental data acquired by [52]. The 3D Finite Element Method was employed to model the experimental system. The 3D Finite Element Method (FEM) employed the macro modelling technique. The DIANA FEA program was employed in the finite element analysis of the wall. The Total Strain Base Crack model was used to simulate the nonlinear material behavior of the wall. Section 3 provides a thorough explanation of the entire total strain base crack model. The wall's linear material properties were derived from [52]. The methodology described in Section 3 was employed to compute the non-linear material properties. The nonlinearity of the wall's material and CFRP are described in detail in Tab. 8. Mechanical properties of CFRP were taken from [52, 53].

Table 8 Homogenized material properties of validation masonry wall and CFRP

Property	Wall	CFRP
E (MPa)	450	230000
F_c (MPa)	1.1	-
F_t (MPa)	0.12	3450
γ_{mas} / g/cm^3	2.0	1.75
v	0.20	0.30
G_c	8	-
G_f	0.09	-
Ultimate Deformation ε / %	-	1.5

The CFRP reinforcement was simulated by employing shell elements that were directly linked to the nodes of the mesh of the panels, without the need for interface elements. The decision to refrain from utilizing interface features may be subject to scrutiny, but it is based on empirical data from experiments. The FRP wrapping system employed in the experiments, along with the surface treatment of the panels, successfully ensured sufficient attachment of the FRP to the support until a significant lateral displacement occurred.

Concise Overview of Experimental Study Used as References

The suggested modeling technique is validated by a series of direct comparisons of the structural response using experimental tests conducted on in-plane-loaded masonry walls by [52]. The horizontal reinforcement was implemented using a U-wrap pattern, with a precise spacing of 526 mm. The as-built panels are classified as P1. CFRP reinforced panels are identified C3. C3 refers to the process of retrofitting using CFRP (carbon fiber reinforced polymer) with a density grid design (Fig. 21).

Finite element models of P1 and C3 were given in Fig. 22.

The calculated force-displacement capacity curve in Fig. 23a is accurately positioned inside the experimental envelope, indicating a high level of representativeness. Specifically, the beginning gradient of the numerical curves closely matches the experimental data, indicating that the numerical elastic stiffness is similar to the actual stiffness. The global force-displacement curves derived for the FRP-reinforced panels (C3) were found to closely match the experimental ones, similar to the unreinforced case (Fig. 23b).

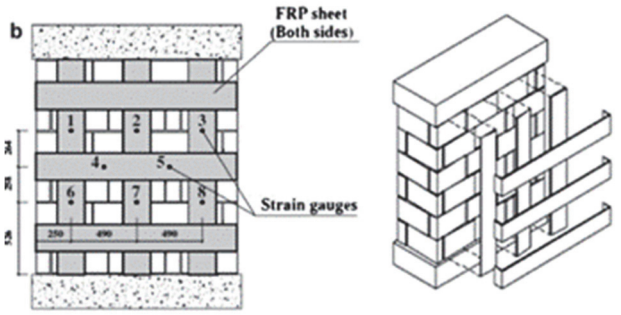

Figure 21 Grid layout of experimental wall

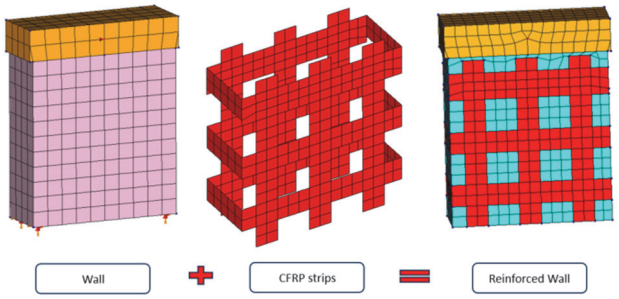

Figure 22 Finite element models of experimental system

Fig. 23 highlights the differences between numerical and experimental outcomes in response curves. Although the overall trend and ultimate capacity align, the model falls short in estimating initial stiffness and slightly overestimates residual strength post-cracking. These variations arise from several factors: Material properties: The strength of the mortar and bond behavior were not field-measured; instead, literature-based values were used, which might not accurately reflect the actual wall properties. Link elements: The macro-model assumed a rigid connection between masonry and CFRP/steel strips, whereas, in reality, local slip and imperfect adhesion could reduce efficiency. End boundary conditions: Experimental supports introduce partial rotations and out-of-plane effects that are simplified in the numerical model. Despite these differences being within 12-18% of benchmark values, better calibration could be achieved by incorporating measured mortar properties, adjusting interface elements for partial slip, and refining boundary condition modeling to enhance the correlation between experimental and numerical behavior.

The cracking propagation was illustrated in Figs. 24a and 24b, both in the experimental and numerical studies. Based on Figs. 24a and 24b, the computational findings showed fracture propagation that was comparable to the experimental data. Upon examination of the data, it is observed that the discrepancies between experimental studies and numerical analyses are insignificant. Therefore, the numerical modeling approach of this reinforcement system may be applied to the structure in the case study.

Table 9 Comparison of experimental and numerical results

P1 (Unreinforced wall)			
	Experimental (mean)	Numerical	Difference / %
Peak displacement / mm	16	18	12.5
Peak Force / kN	132	111	15.9
C3 (Reinforced wall (grid pattern)			
	Experimental	Numerical	Difference
Peak displacement / mm	27.5	26.7	2.9
Peak Force / kN	198.2	188	5.1

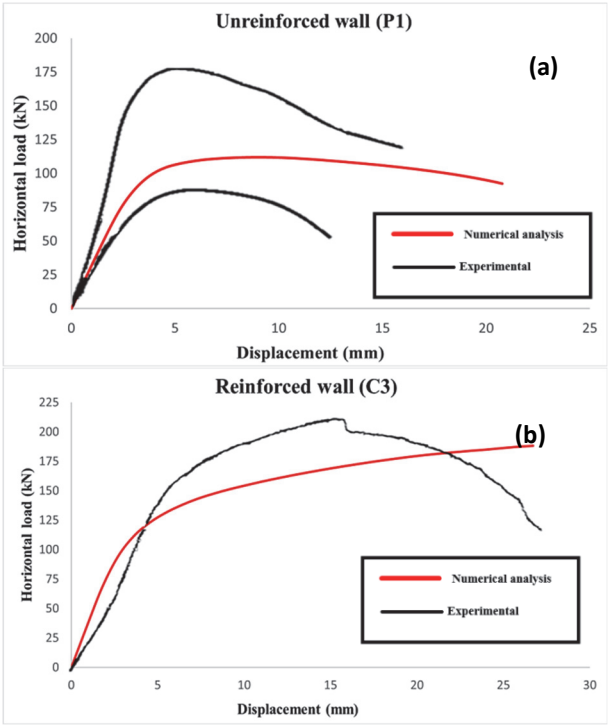

Figure 23 The force-displacement capacity curves of experimental and numerical analysis

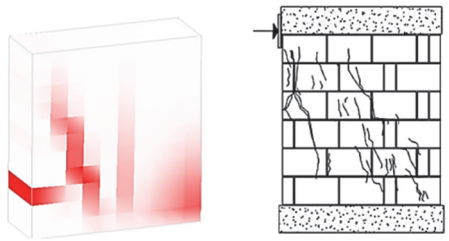

Figure 24a Crack propagation of the wall for P1

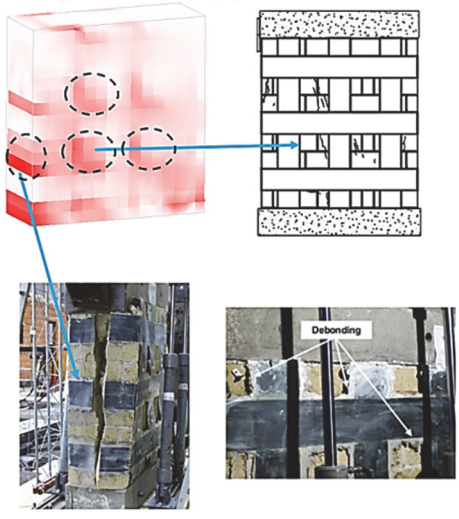

Figure 24b Crack propagation of the wall for C3

6 RETROFITTED STATE RESULTS OF THE BUILDING

According to the nonlinear time history analyses results obtained in Section 4, locations of crack propagation were given in Fig. 14. It is seen that tensile damages occurred in the walls marked in Fig. 15. For this reason, the retrofitting methods described in detail in the section 5.1 and 5.2 were applied to these walls. In this section, the retrofit methods discussed in this study are numerically applied to the building and the change in the seismic performance of the structure is observed.

6.1 Retrofitted Case of the Building with Stainless Steel

The 3D numerical representation of the Stainless-Steel retrofitted model is seen in Fig. 25. The retrofitted structure's 3D finite element model has 217034 elements and 108589 nodes. The retrofit method was applied to the ground floor and first floor as critical cracks had developed on the first two floors. The reinforced structural model underwent pushover and non-linear time history studies. Since the weak direction of the structure is along the y-axis, pushover analysis was performed on the y-axis (longitudinal direction). Fig. 26 displays the capacity curves for both the existing structure and the reinforced structure. The load capacity in the longitudinal direction has increased from 0.45 g to 0.69 g. Furthermore, the displacement capabilities were enhanced. The non-linear time history analysis also showed significant improvements in the reinforced structure's performance, with reduced deformations and increased overall stability (Fig. 26 and Tab. 10). The reinforcement measures taken on the ground floor and first floor have successfully strengthened the building's ability to withstand seismic forces in the *y*-axis direction. The capacity curves clearly demonstrate the positive impact of the structural enhancements, providing reassurance of the building's improved resilience against future earthquakes.

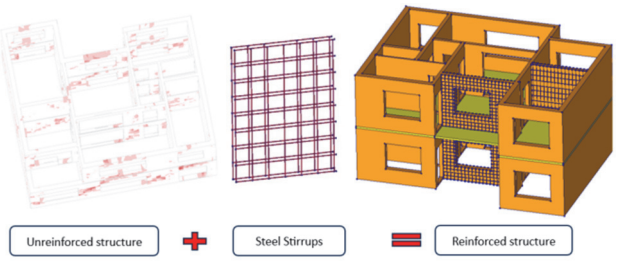

Figure 25 Retrofitting scheme and FEM of reinforced structure

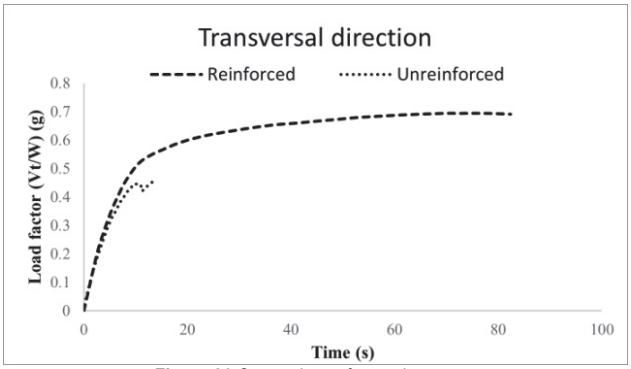

Figure 26 Comparison of capacity curves

The 2023 Doğanşehir earthquake resulted in the highest normalized displacement, maximum crack width,

and inter-story drift ratio for the unreinforced structure. Therefore, the nonlinear time history analyses utilized the seismic records from the 2023 Doğanşehir earthquake for the stainless-steel reinforced structure.

The building was subjected to earthquake recordings with an effective duration of 15 seconds in the *y* direction. The time history analysis was used to determine the maximum normalized displacement, maximum crack width, and maximum inter-story drift ratio. These values were then compared to the findings obtained from the time history analysis of the structure without reinforcement. Comparison of the findings from nonlinear time history analysis is shown in Tab. 10. Furthermore, Fig. 27 displays the distribution of crack width at the conclusion of the time history study during the 2023 Doğanşehir earthquake.

Table 10 Comparation of the nonlinear time history analyses results

	2023 Doğanşehir earthquake		
	Unreinforced	Reinforced	Difference / %
Normalized displacement / %	0.44	0.42	4.55
Max. Crack width / mm	15.24	10.86	28.74
Max. inter story Drift ratio / %	0.48	0.42	10.42

The Doğanşehir earthquake of 2023 was analyzed through nonlinear time history analyses, with a focus on comparing the results between unreinforced and reinforced structures. The results indicated a slight reduction in parameters such as normalized displacement and inter-story drift ratio, while a substantial reduction in crack width was observed in the reinforced structure. The outcome is attributed to the fact that the strengthening methods used, such as stainless-steel strips and CFRP laminates, primarily function at a local level by confining masonry units and bridging cracks, rather than significantly enhancing the overall stiffness of the structure. Consequently, reductions in inter-storey drift and displacement are minimal, but crack propagation is effectively managed, resulting in much narrower crack widths. This suggests that the retrofitting techniques mainly improve damage control and reparability rather than significantly boosting the structure's overall deformation capacity.

This suggests that the reinforcement measures implemented were effective in reducing the structural vulnerability to seismic events. The responses of the story added building (unreinforced) remained above the Collapse prevention (CP) performance level according to FEMA 356. The performance level of the retrofitted structure was between Life Safety (LS) and Collapse Prevention (CP) (significant but restorable damage).

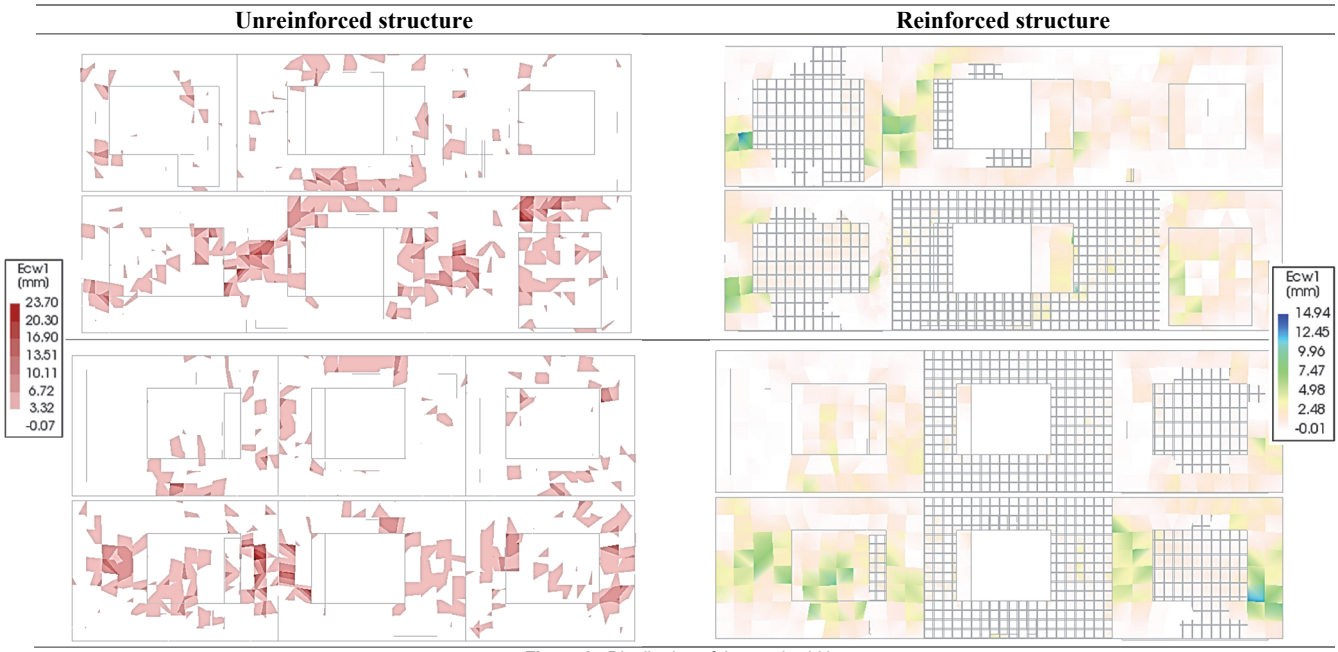

Figure 27 Distribution of the crack widths

While the selected retrofitting method has not changed the dynamic response of the structure, it decreased the amplitudes related to the seismic vulnerability of the structure. In addition, this method has not increased the mass of the structure. Therefore, this method is easily applicable and effective in improving the seismic resistance of the structure. In practical applications, once the retrofitting systems such as steel strips or CFRP laminates are installed, the walls are not left exposed as depicted in Figs. 17 and 20. Instead, a thin layer of mortar or plaster is usually reapplied for both protection and aesthetic purposes. This additional layer adds only a minimal amount of structural mass in comparison to the overall mass of the wall. Consequently, in our models, the final layer of mortar or plaster was not explicitly included, and its mass effect was disregarded, as it does not have a significant impact on the overall seismic response of the structure.

6.2 Retrofitted Case of the Building with CFRP

The 3D numerical representation of the CFRP retrofitted model is seen in Fig. 28. The retrofitted structure's 3D finite element model has 431952 elements and 166839 nodes. The retrofit method was applied to the ground floor and first floor as critical cracks had developed

on the first two floors. The reinforced structural model underwent pushover and non-linear time history analysis. Since the weak direction of the structure is along the *y*-axis, pushover analysis and NLTH analysis were performed on the *y*-axis (longitudinal direction).

Fig. 29 displays the capacity curves for both the existing structure (story added building) and the CFRP reinforced structure. The load capacity in the longitudinal direction has increased from 0.45 g to 0.79 g. Furthermore, the displacement capabilities were enhanced. The addition of CFRP reinforcement has significantly improved the structural performance of the building, increasing both load capacity and displacement capabilities in the longitudinal direction. This demonstrates the effectiveness of using CFRP reinforcement in enhancing the seismic resilience of structures.

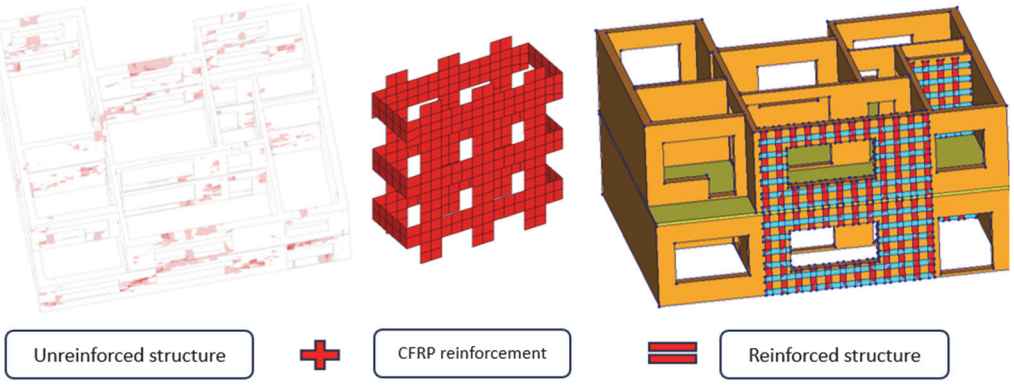

Figure 28 FEM of CFRP reinforced structure

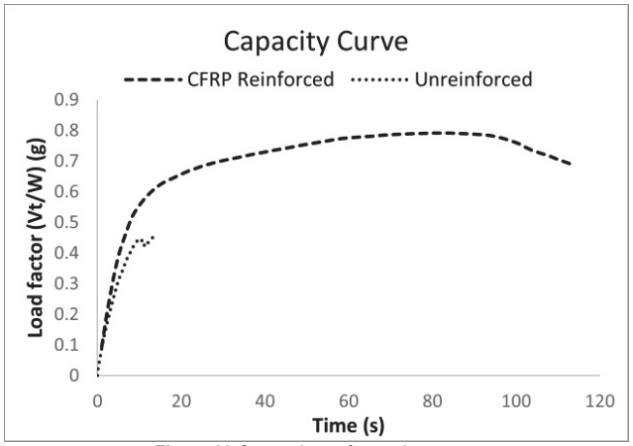

Figure 29 Comparison of capacity curves

The 2023 Doğanşehir earthquake resulted in the highest normalized displacement, maximum crack width and inter-story drift ratio for the unreinforced structure. Therefore, the nonlinear time history analyses utilized the seismic records from the 2023 Doğanşehir earthquake for the CFRP reinforced structure. The building was subjected to earthquake recordings with an effective duration of 15 seconds in the y direction. The time history analysis was used to determine the maximum normalized displacement, maximum crack width, and maximum inter-story drift ratio. These values were then compared to the findings obtained from the time history analysis of the structure without reinforcement. Comparison of the findings from nonlinear time history analysis is shown in Tab. 11. Furthermore, Fig. 30 displays the distribution of crack width at the last of the time history analysis during the 2023 Doğanşehir earthquake.

According to the results of the nonlinear time history analyses, the maximum normalized displacement, maximum crack width, and maximum inter-story drift ratio values decreased in the CFRP reinforced structure. The responses of the building (unreinforced) remained above the Collapse prevention (CP) performance level according to FEMA 356. The performance level of the retrofitted structure was between Life Safety (LS) and Collapse Prevention (CP) (significant but restorable damage).

Table 11 Comparison of the nonlinear time history analyses results

	2023 Doğanşehir earthquake		
	Unreinforced	Reinforced	Difference / %
Normalized displacement / %	0.33	0.30	9.09
Max. Crack width / mm	15.24	11.11	27.10
Max. inter story Drift ratio / %	0.48	0.39	18.75

While the selected retrofitting method has not changed the dynamic response of the structure, it decreased the amplitudes related to the seismic vulnerability of the structure. In addition, this method has not increased the mass of the structure. Therefore, this method is easily applicable and effective in improving seismic resistance of the structure. After retrofitting, crack widths decreased and crack accumulation occurred in the *x*-direction walls that were not retrofitted. The occurrence of cracks in the reinforced walls is quite low. When both retrofitting methods were compared, the load bearing capacity and displacement limits of the structure increased more in the retrofitting with CFRP application. Overall, retrofitting with CFRP application proved to be more effective in improving the seismic resistance of the structure compared to steel stirrup methods. The decrease in crack widths and low occurrence of cracks in reinforced walls further support the success of this method.

This research relies entirely on numerical simulations, with experimental validation sourced from existing tests on comparable masonry systems. To facilitate the practical application of the suggested retrofitting techniques and bolster confidence in policy and design, several verification steps are advised. Laboratory experiments on representative wall panels enhanced with stainless-steel strips or CFRP should be performed to assess crack progression, ultimate capacity, drift, and bond behavior. At the subassembly and building level, pilot retrofits of wall

piers or bays can yield short-term monitoring data under ambient or minor seismic conditions. Ultimately, shake-table tests of full-scale specimens and long-term health monitoring of retrofitted structures would reinforce the evidence base. The study has certain limitations: mortar properties were derived from literature rather than measured on-site, interfaces were assumed to be perfect bonds, and boundary conditions and out-of-plane effects were simplified. Additionally, the re-applied plaster layer post-retrofitting was not explicitly modeled, as its added mass was deemed negligible. Future research should thus concentrate on project-specific material testing, calibration of interface models to permit partial slip, parametric studies on strip/CFRP spacing and anchorage, and assessment of out-of-plane stability and fire sensitivity of CFRP. These steps will ensure that the proposed strengthening methods can be experimentally validated and effectively translated into practice.

Figure 30 Distribution of and crack width

8 CONCLUSIONS

This study examines the seismic performance of a masonry residential building that collapsed following the 6 February 2023 Kahramanmaraş earthquakes in Türkiye, focusing on a case study located in Malatya province. The structural performance of the building was assessed in its retrofitted state, employing various reinforcement techniques in a numerical model to enhance its earthquake resistance. To evaluate the building's seismic behavior, both nonlinear static (pushover) and nonlinear dynamic (time history) analyses were conducted, providing insights into its performance under different seismic loading scenarios.

According to the analyses results:

- Based on the acceptance criteria, the responses of the unreinforced building remained above the Collapse prevention (CP) performance level (near collapse).
- When applying the steel stirrup retrofitting technique, the load capacity in the longitudinal direction has enhanced from 0.45 g to 0.69 g. Furthermore, the displacement capabilities were enhanced. Additionally, according to the NLTHA of steel stirrup retrofitted building, normalized displacement was decreased as 4.55%, max. Crack width was decreased as 28.7%.
- When applying the CFRP retrofitting technique, the load capacity in the longitudinal direction has increased from 0.45 g to 0.79 g. Furthermore, the displacement capabilities were enhanced. In addition, according to the NLTHA of CFRP retrofitted building, normalized displacement was decreased as 9.09%, max. crack width was decreased as 27.1% and max. inter story Drift ratio was decreased as 18.75%.
- When both retrofitting methods were compared, the load bearing capacity and displacement limits of the structure more increased in the retrofitting with CFRP application.

Turkey is located in a region that is constantly threatened by earthquakes. Hence, the seismic performance of structures should be investigated. In addition, if the level of performance required by the local seismic code has not been met, a retrofitting method should be considered, and a numerical FE analysis of the retrofit case should be performed.

Acknowledgments

The author thanks to Malatya Metropolitan Municipality and Malatya Battalgazi Municipality for the information provided about the building.

9 REFERENCES

[1] İnce, O. (2024). Structural damage assessment of reinforced concrete buildings in Adıyaman after Kahramanmaraş (Türkiye) Earthquakes on 6 February 2023. *Engineering Failure Analysis*, *156*, 107799. https://doi.org/10.1016/j.engfailanal.2023.107799

[2] Ozturk, M., Arslan, M. H., & Korkmaz, H. H. (2023). Effect on RC buildings of 6 February 2023 Turkey earthquake doublets and new doctrines for seismic design. *Engineering Failure Analysis*, *153*, 107521. https://doi.org/10.1016/j.engfailanal.2023.107521

[3] Sezgin, S. K., Sakcalı, G. B., Özen, S., Yıldırım, E., Avcı, E., Bayhan, B., & Çağlar, N. (2024). Reconnaissance report on damage caused by the February 6, 2023, Kahramanmaraş Earthquakes in reinforced-concrete structures. *Journal of Building Engineering*, *89*, 109200. https://doi.org/10.1016/j.jobe.2024.109200

[4] Vuran, E., Serhatoğlu, C., Timurağaoğlu, M. Ö., Smyrou, E., Bal, İ. E., & Livaoğlu, R. (2024). Damage observations of RC buildings from 2023 Kahramanmaraş earthquake sequence and discussion on the seismic code regulations. *Bulletin of Earthquake Engineering*, 1-30. https://doi.org/10.1007/s10518-023-01843-3

[5] Doğan, T. P., Kalkan, H., Aldemir, Ö., Ayhan, M., Böcek, M., & Anıl, Ö. (2024). Investigation of RC structure damages after February 6, 2023, Kahramanmaraş earthquake in the Hatay region. *Bulletin of Earthquake Engineering*, 1-29. https://doi.org/10.1007/s10518-024-01965-2

[6] Binici, B., Yakut, A., Kadas, K., Demirel, O., Akpinar, U., Canbolat, A., Yurtseven, F., Oztaskin, O., Aktas, S., & Canbay, E. (2023). Performance of RC buildings after Kahramanmaraş earthquakes: lessons toward performance based design. *Earthquake Engineering and Engineering Vibration*, *22*(4), 883-894. https://doi.org/10.1007/s11803-023-2206-8

[7] Mertol, H. C., Tunç, G., Akış, T., Kantekin, Y., & Aydın, İ. C. (2023). Investigation of RC buildings after 6 February 2023, Kahramanmaraş, Türkiye earthquakes. *Buildings*, *13*(7), 1789. https://doi.org/10.3390/buildings13071789

[8] Işık, E., Avcil, F., Büyüksaraç, A., İzol, R., Arslan, M. H., Aksoylu, C., Harirchian, E., Eyisüren, O., Arkan, E., & Güngür, M. Ş. (2023). Structural damages in masonry buildings in Adıyaman during the Kahramanmaraş (Turkiye) earthquakes (Mw 7.7 and Mw 7.6) on 06 February 2023. *Engineering Failure Analysis*, *151*, 107405. https://doi.org/10.1016/j.engfailanal.2023.107405

[9] Kahya, V., Genç, A. F., Sunca, F., Roudane, B., Altunişik, A. C., Yilmaz, S., Günaydin, M., Dok, G., Kirtel, O., & Demir, A. (2024). Evaluation of earthquake-related damages on masonry structures due to the 6 February 2023 Kahramanmaraş-Türkiye earthquakes: A case study for Hatay Governorship Building. *Engineering Failure Analysis*, *156*, 107855. https://doi.org/10.1016/j.engfailanal.2023.107855

[10] Mercimek, Ö. (2023). Seismic failure modes of masonry structures exposed to Kahramanmaraş earthquakes (Mw 7.7 and 7.6) on February 6, 2023. *Engineering Failure Analysis*, *151*, 107422. https://doi.org/10.1016/j.engfailanal.2023.107422

[11] Işık, E., Avcil, F., Arkan, E., Büyüksaraç, A., İzol, R., & Topalan, M. (2023). Structural damage evaluation of mosques and minarets in Adıyaman due to the 06 February 2023 Kahramanmaraş earthquakes. *Engineering Failure Analysis*, *151*, 107345. https://doi.org/10.1016/j.engfailanal.2023.107345

[12] Çağlar, H., Çağlar, A., Korkmaz, S. Z., Demirel, B., & Bayraktar, O. Y. (2018). Geleneksel Kastamonu Evlerinin İnşasında Kullanılan El İle Üretilmiş Harman Tuğla İle Fabrikasyon Olarak Üretilen Tuğlanın Fiziksel, Mekanik Ve Yapısal Karakterizasyon Özelliklerinin Karşılaştırılması. *Fırat Üniversitesi Mühendislik Bilimleri Dergisi*, *30*(2), 39-48.

[13] Lourenco, P. (1996). Computational Strategy for Masonry *Structures*. PhD Thesis, Delft Technical University of Technology.

[14] Carpinteri, A., Invernizzi, S., & Lacidogna, G. (2005). In situ damage assessment and nonlinear modelling of a historical masonry tower. *Engineering Structures*, *27*(3), 387-395. https://doi.org/10.1016/j.engstruct.2004.11.001

[15] Özmen, A. & Sayın, E. (2023). 3D Soil Structure Interaction Effects on the Seismic Behavior of Single Span Historical Masonry Bridge. *Geotechnical and Geological Engineering*, *41*(3). https://doi.org/10.1007/s10706-023-02389-6

[16] Hökelekli, E. & Al-Helwani, A. (2020). Effect of soil properties on the seismic damage assessment of historical masonry minaret–soil interaction systems. *The Structural Design of Tall and Special Buildings*, *29*(2), e1694. https://doi.org/10.1002/tal.1694

[17] Onat, O., Deniz, F., Özmen, A., Özdemir, E., & Sayın, E. (2023). Performance evaluation and damage assessment of historical Yusuf Ziya Pasha Mosque after February 6, 2023 Kahramanmaras earthquakes. *Structures*, *58*, 105415. https://doi.org/10.1016/j.istruc.2023.105415

[18] Kocaman, İ. & Kazaz, İ. (2023). Collapse mechanism of historical masonry mosques under strong ground motions. *Engineering Failure Analysis*, *144*, 106983. https://doi.org/10.1016/j.engfailanal.2022.106983

[19] Bilgin, H., Shkodrani, N., Hysenlliu, M., Ozmen, H. B., Isik, E., & Harirchian, E. (2022). Damage and performance evaluation of masonry buildings constructed in 1970s during the 2019 Albania earthquakes. *Engineering Failure Analysis*, *131*, 105824. https://doi.org/10.1016/j.engfailanal.2021.105824

[20] Kocaman, İ. & Kazaz, İ. (2023). Global drift ratio limits for historical masonry mosques. *Bulletin of Earthquake Engineering*, *21*(5), 3011-3040. https://doi.org/10.1007/s10518-023-01613-1

[21] Gönen, S. & Soyöz, S. (2021). Seismic analysis of a masonry arch bridge using multiple methodologies. *Engineering Structures*, *226*, 111354. https://doi.org/10.1016/j.engstruct.2020.111354

[22] Proske, D. & Van Gelder, P. (2009). *Safety of historical stone arch bridges*. Springer Science & Business Media. https://doi.org/10.1007/978-3-540-77618-5

[23] Guideline for Load and Resistance Assessment of Existing European Railway Bridges: Advices on the Use of Advanced Methods, COWI A/S (2007).

[24] Baykasoğlu, A., Güllü, H., Çanakçı, H., & Özbakır, L. (2008). Prediction of compressive and tensile strength of limestone via genetic programming. *Expert Systems with Applications*, *35*(1-2), 111-123. https://doi.org/10.1016/j.eswa.2007.06.006

[25] Bayraktar, A. & Hökelekli, E. (2021). Nonlinear soil deformability effects on the seismic damage mechanisms of brick and stone masonry arch bridges. *International Journal of Damage Mechanics*, *30*(3), 431-452. https://doi.org/10.1177/1056789520974423

[26] Karaton, M., Aksoy, H. S., Sayın, E., & Calayır, Y. (2017). Nonlinear seismic performance of a 12th century historical masonry bridge under different earthquake levels. *Engineering Failure Analysis*, *79*, 408-421. https://doi.org/10.1016/j.engfailanal.2017.05.017

[27] Ersoy, H. Y. (2001). *Composite material*. Literature, Istanbul, Turkey.

[28] Eurocode 6. (2005). *Design of masonry structures - part 1-1: General rules for reinforced and unreinforced masonry structures*. Comité Européen de Normalisation: Brussels, Belgium.

[29] Vecchio, F. J. & Collins, M. P. (1986). The modified compression-field theory for reinforced concrete elements subjected to shear. *ACI J.*, *83*(2), 219-231. https://doi.org/10.14359/10416

[30] DIANA FEA. (2022). *User's Manual Release 10.5*. The Netherlands.

[31] Lourenço, P. B. & Pereira, J. M. (2018). *Seismic retrofitting project: recommendations for advanced modeling of historic earthen sites*. Getty Conservation Institute.
[32] Krejčí, T., Koudelka, T., Bernardo, V., & Šejnoha, M. (2021). Effective elastic and fracture properties of regular and irregular masonry from nonlinear homogenization. *Computers & Structures*, *254*, 106580. https://doi.org/10.1016/j.compstruc.2021.106580
[33] Valente, M. & Milani, G. (2018). Seismic response and damage patterns of masonry churches: seven case studies in Ferrara, Italy. *Engineering Structures*, *177*, 809-835. https://doi.org/10.1016/j.engstruct.2018.08.071
[34] Chopra, A. K. & Goel, R. K. (2002). A modal pushover analysis procedure for estimating seismic demands for buildings. *Earthquake Engineering & Structural Dynamics*, *31*(3), 561-582. https://doi.org/10.1002/eqe.144
[35] Minghini, F., Bertolesi, E., del Grosso, A., Milani, G., & Tralli, A. (2016). Modal pushover and response history analyses of a masonry chimney before and after shortening. *Engineering Structures*, *110*, 307-324. https://doi.org/10.1016/j.engstruct.2015.11.016
[36] Tiberti, S., Acito, M., & Milani, G. (2016). Comprehensive FE numerical insight into Finale Emilia Castle behavior under 2012 Emilia Romagna seismic sequence: Damage causes and seismic vulnerability mitigation hypothesis. *Engineering Structures*, *117*, 397-421. https://doi.org/10.1016/j.engstruct.2016.02.048
[37] Mendes, N. (2012). *Seismic assessment of ancient masonry buildings: shaking table tests and numerical analysis*. PhD Thesis, Universidade do Minho.
[38] Afetve Acil Durum Yönetimi Başkanlığı (2020).
[39] Rathje, E. M., Faraj, F., Russell, S., & Bray, J. D. (2004). Empirical relationships for frequency content parameters of earthquake ground motions. *Earthquake Spectra*, *20*(1), 119-144. https://doi.org/10.1193/1.1643356
[40] McGuire, R. K. (1978). Seismic ground motion parameter relations. *Journal of the Geotechnical Engineering Division*, *104*(4), 481-490. https://doi.org/10.1061/AJGEB6.0000615
[41] Tso, W. K., Zhu, T. J., & Heidebrecht, A. C. (1992). Engineering implication of ground motion A/V ratio. *Soil Dynamics and Earthquake Engineering*, *11*(3), 133-144. https://doi.org/10.1016/0267-7261(92)90027-B
[42] Turkish Building Earthquake Code 2018, Disaster and Emergency Management Agency (AFAD) (2018).
[43] Seismomatch. (2021). Earthquake software for response spectrum matching. Seismosoft Ltd. https://seismosoft.com
[44] Sayin, E. (2016). Nonlinear seismic response of a masonry arch bridge. *Earthquakes and Structures*, *10*(2), 483-494. https://doi.org/10.12989/eas.2016.10.2.483
[45] Özmen, A. & Sayın, E. (2021). Seismic Response of a Historical Masonry Bridge under Near and Far-fault Ground Motions. *Periodica Polytechnica Civil Engineering*, *65*(3), 946-958. https://doi.org/10.3311/PPci.17832
[46] Altunışık, A. C. & Genç, A. F. (2017). Earthquake response of heavily damaged historical masonry mosques after restoration. *Natural Hazards and Earth System Sciences*, *17*(10), 1811-1821. https://doi.org/10.5194/nhess-17-1811-2017
[47] Pre-Standard and Commentary for the Seismic Rehabilitation of Buildings (2000).
[48] Hancilar, U., Çaktı, E., & Erdik, M. (2012). Earthquake performance assessment and rehabilitation of two historical unreinforced masonry buildings. *Bulletin of Earthquake Engineering*, *10*, 307-330. https://doi.org/10.1007/s10518-011-9281-3
[49] Jin, Y.-H., Zhou, Z.-Y., Bao, B.-L., Wang, H.-Y., & Wang, T. (2023). Experimental study on the seismic performance of clay brick masonry wall strengthened with stainless steel strips. *Journal of Building Engineering*, *69*, 106076. https://doi.org/10.1016/j.jobe.2023.106076
[50] Rahman, A. & Ueda, T. (2016). In-plane shear performance of masonry walls after strengthening by two different FRPs. *Journal of Composites for Construction*, *20*(5), 04016019. https://doi.org/10.1061/(ASCE)CC.1943-5614.0000661
[51] Corradi, M., Osofero, A. I., Borri, A., & Castori, G. (2015). Strengthening of historic masonry structures with composite materials. *Handbook of research on seismic assessment and rehabilitation of historic structures*. IGI Global. https://doi.org/10.4018/978-1-4666-8286-3.ch008
[52] Marcari, G., Manfredi, G., Prota, A., & Pecce, M. (2007). In-plane shear performance of masonry panels strengthened with FRP. *Composites Part B: Engineering*, *38*(7-8), 887-901. https://doi.org/10.1016/j.compositesb.2006.11.004
[53] Gattulli, V., Lampis, G., Marcari, G., & Paolone, A. (2014). Simulations of FRP reinforcement in masonry panels and application to a historic facade. *Engineering Structures*, *75*, 604-618. https://doi.org/10.1016/j.engstruct.2014.06.023

Contact information:

Alper ÖZMEN, Assistant Professor
Faculty of Engineering,
Civil Engineering Department,
Inonu University,
Malatya, Türkiye
E-mail: alper.ozmen@inonu.edu.tr